Rippling Patterns in Aggregates of Myxobacteria Arise from Cell-Cell Collisions

Uwe Börner,[1] Andreas Deutsch,[1,2] Hans Reichenbach,[3] and Markus Bär[1]

[1]*Max Planck Institute for Physics of Complex Systems, Nöthnitzer Straße 38, 01187 Dresden, Germany*
[2]*Zentrum für Hochleistungsrechnen, TU Dresden, Zellescher Weg 12, 01069 Dresden, Germany*
[3]*GBF–Gesellschaft für Biotechnologische Forschung mbH, Abteilung Naturstoffchemie, Mascheroder Weg 1, 38124 Braunschweig, Germany*

(Received 17 July 2001; published 26 July 2002)

Experiments with myxobacterial aggregates reveal standing waves called rippling patterns. Here these structures are modeled with a simple discrete model based on the interplay between migration and collisions of cells. Head-to-head collisions of cells result in cell reversals. To correctly reproduce the rippling patterns, a refractory phase after each cell reversal has to be assumed, during which further reversal is prohibited. The duration of this phase determines the wavelength and period of the ripple patterns as well as the reversal frequency of single cells.

DOI: 10.1103/PhysRevLett.89.078101 PACS numbers: 87.18.Ed, 05.65.+b, 87.18.Hf

Introduction.—Pattern formation in aggregates of bacteria and amoebae is a widely observed phenomenon [1]. Complex colonial patterns of spots, stripes, and rings are produced by *E. coli* [2]. *Bacillus subtilis* exhibits branching patterns during colonial growth [3]. Two- and three-dimensional circular waves and spirals have been observed during aggregation of *Dictyostelium discoideum* [4–7], often closely resembling patterns in chemical reactions [8]. These patterns are typically modeled with continuous reaction-diffusion equations describing the spatiotemporal evolution of the cell density and concentrations of chemoattractants and nutrients, e.g., for *Dictyostelium discoideum* [1,9,10] and *E. coli* [11,12]. An alternative approach uses discrete models that describe the motion of individual cells and swarm formation [13–15]. Myxobacteria [16,17] provide one of the most intriguing examples for morphogenesis and pattern formation. As long as there is a sufficient food supply, vegetative cells grow and divide. But when nutrients run short, bacteria aggregate and finally build a multicellular structure, the fruiting body.

Myxobacterial rippling.—Fruiting body formation is often preceded by a periodic pattern originally classified as *oscillatory waves* and later named *rippling*. Rippling is found in myxobacteria such as *Myxococcus xanthus* [18–20]. An experimental illustration of the rippling phenomenon is shown in Fig. 1(a). Bacteria organize into equally spaced ridges (dark regions) that are separated by regions with low cell density (light regions). We examine the temporal dynamics of the density profile along a one-dimensional cut indicated by the white line in Fig. 1(a). The resulting space-time plot reveals a periodically oscillating standing wave pattern [Fig. 1(b)]. To model the formation of rippling patterns is a significant first step in the understanding of the life cycle of myxobacteria. Several experimental studies [18–20] report periodic rippling patterns with wavelengths between 45 and 90 μm, wave velocities between 2 and 11 $\mu\mathrm{m\,min}^{-1}$, and temporal periods between 10 and 20 min. Typical cell lengths vary between 5 and 10 μm, so that the rippling wavelength corresponds to 10–20 cell lengths. In addition, single cells have been found to move unidirectionally with the ripple waves in a typical back and forth manner; they reverse their direction of motion with a mean reversal frequency of about 0.1 reversals min^{-1}.

Model.—In the following, we present a discrete model for the formation of ripple patterns which is based on the dynamics of single cells. Our model is defined on a fixed square lattice in the x-y plane and assumes discrete space coordinates, analogous to cellular automaton models. The discrete z coordinate describes the number of cells piled up on top of each other in a given lattice point in the x-y plane [Fig. 2(a)]. The spatial lattice constants are chosen according to the size of a bacterial cell (≈ 6 μm) in the x and (≈ 1 μm) in the y and z directions.

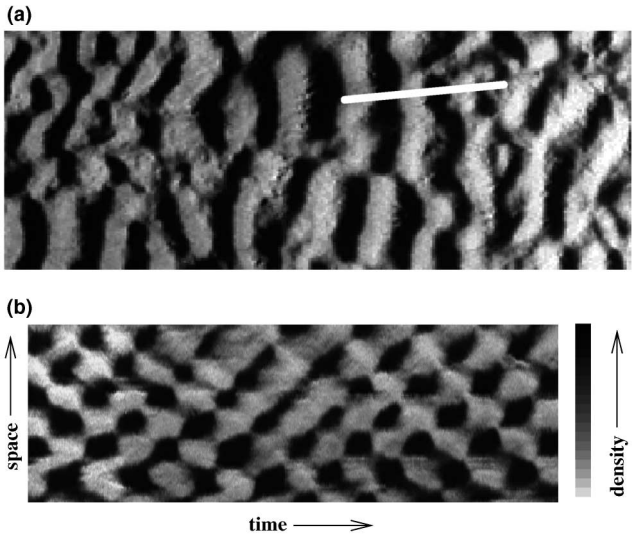

FIG. 1. (a) Snapshot from a rippling sequence in myxobacteria taken from a time-lapse movie. White bar: 300 μm. (b) Space-time plot of the density profile along the white line in (a). Wavelength is 105 μm, temporal period is 10 min.

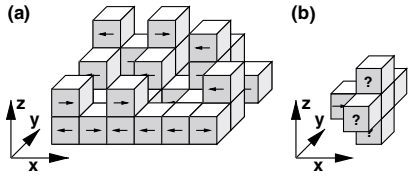

FIG. 2. (a) Exemplary configuration of the model; the cell orientation is indicated by arrows. (b) The interaction neighborhood is a five nodes cross in the y-z plane at that x position the cell is directed to (here the cell orientation is the $+x$ direction).

The basic rules of the model are derived from the experimental results by Sager and Kaiser [20]: Within the rippling phase, cells are found to move on linear paths parallel to each other about a distance of one wavelength. When two opposite moving cells collide head-on, they reverse their gliding direction due to the exchange of a small, membrane-associated protein called C-factor. Furthermore, we assume a refractory phase of duration τ in which cells cannot respond to C-signal, and reversal is prohibited. τ is the most relevant control parameter.

The number of cells is constant (absence of cell replication and death); i.e., the average height (average number of cells per lattice site) $\bar{n}$ is a second parameter in the model. All cells are assumed identical with respect to length, velocity, and duration of the refractory phase. This simplifies the analysis considerably. We have, however, tested that the results presented below are robust to small variations in duration of refractory phases and velocities that are expected in the experimental system. Large variations of any of these quantities, however, prevent formation of the rippling patterns.

Because rippling cells mainly move on linear paths, we studied also a two-dimensional (2D) model in the x-z plane. Nevertheless, the three-dimensional (3D) case is closer to the experimental situation. In the 3D model, movement of individual bacteria is restricted to sheets with a fixed y coordinate, assuming that alignment of cells takes place before the onset of rippling. The coupling in the y direction is solely due to interaction. A single cell is thus described by a three-dimensional space coordinate (x, y, z) and an orientation variable $\phi \in \{-1(\text{left}), 1(\text{right})\}$ referring to the gliding direction.

Cells interact solely via head-on collisions; i.e., cells only sense counterpropagating cells in a certain interaction neighborhood. When a sensitive cell collides head-on with other cells (the meaning of collisions will be specified below), it reverses its gliding direction and is temporarily refractory. The sensitivity of a bacterium to C-factor is described by a *clock* variable ν which measures the time since the last reversal; thus a cell with $\nu < \tau$ is insensitive to C-factor.

The temporal update of the model consists of a migration and an interaction step and is performed in discrete steps; the step size reflects the time a cell needs to advance by one cell length (≈ 1 min). In the asynchronous migration step, cells move according to their orientation to the neighboring site in the x direction. If this site is already occupied, the cell pushes its way between cells of the next column and slips beneath or above the blocking cell with equal probability. Cells are assumed to rest with small probabilities $p \leq 0.05$. Interaction takes place simultaneously; in 3D every sensitive cell ($\nu \geq \tau$) checks a neighborhood of five nodes depending on its orientation ϕ [Fig. 2(b)]. If a cell encounters at least one cell with opposite orientation in this neighborhood in its direction of motion (*collision*), the cell reverses orientation ($\phi \rightarrow -\phi$) and will be refractory for $\tau - 1$ time steps. In the 2D model, sensitive cells reverse only upon head-on collision with cells at the same level (one-node interaction neighborhood). Insensitive refractory cells cannot reverse due to collisions, but still can cause the reversal of other sensitive cells. Random initial conditions and periodic boundary conditions are used throughout the simulations.

Simulation results.—We performed systematic simulations by varying the two model parameters τ and $\bar{n}$. The results depend only weakly on the number of cells in the aggregate; variations of the average number $\bar{n}$ of cells per lattice point between 2 and 10 do not produce significant changes; results presented here are for $\bar{n} = 3$. The duration of the refractory phase τ is the decisive quantity for pattern formation. If there is no refractory period, all collisions lead to reversal of both involved cells and do not change the densities of left- and right-moving cells. If a refractory cell and a sensitive cell collide, only the latter will reverse and both cells move in the same direction. This provides the microscopic symmetry breaking which is necessary (but not sufficient) for the emergence of the macroscopic rippling patterns.

Our simulations show that refractory times below a certain threshold do not lead to a visible rippling pattern [see Figs. 3(a) and 3(b)]. If the refractory phase is longer than 2 min, we can, however, extract a typical length scale by spatial Fourier transformation. For sufficiently long refractory time τ, the rippling pattern and the temporal evolution obtained in the model [Figs. 3(c) and 3(d)] are in good agreement with the experimental data of Fig. 1. Waves propagate equally in both directions; their superposition forms a standing wave. The pattern is easily recognizable—wavelength and period of the ripples have been reproduced in several independent runs.

Wavelength and temporal period of the ripple pattern increase with the duration τ of the refractory phase [see Figs. 4(a) and 4(b)]. In 3D, wavelength and temporal period are up to 20% smaller than in 2D [see Figs. 4(a) and 4(b)]. The experimental values of wavelength and temporal period of the rippling pattern are reproduced with refractory times of 4–5 min. The 3D model also shows straightening of the ripples in the course of the simulations.

The discrete model enables us to track the single cell behavior. Typically, cells move over a distance of about

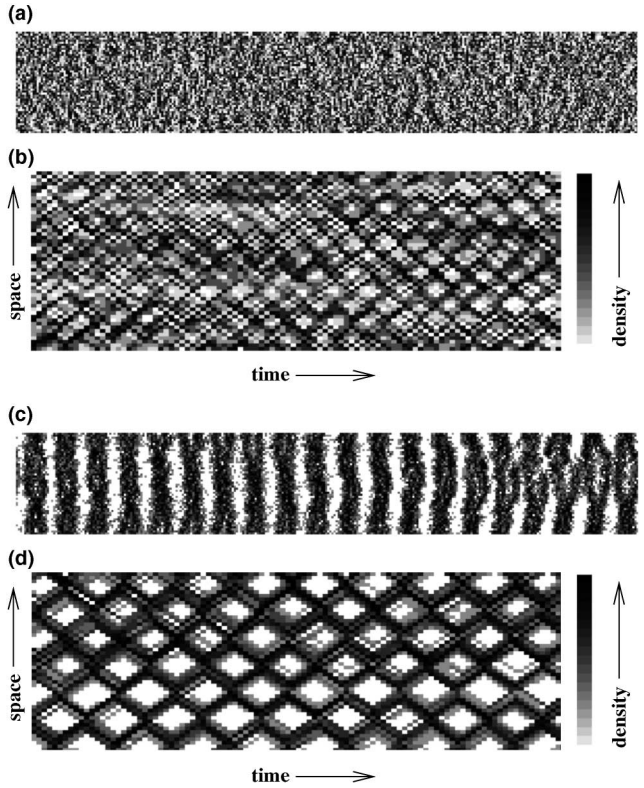

FIG. 3. (a) Simulation snapshot in a system of size 300×50 with a refractory phase $\tau = 3$ min after ca. 2000 time steps and (b) corresponding space-time plot of the height profile (black corresponds to high columns) along 50 lattice sites in the x direction over 100 time steps. One can recognize a noise-induced pattern without long-range correlations. (c),(d) Same as (a),(b) but with a refractory phase $\tau = 5$ min. The pattern is now very regular and stable.

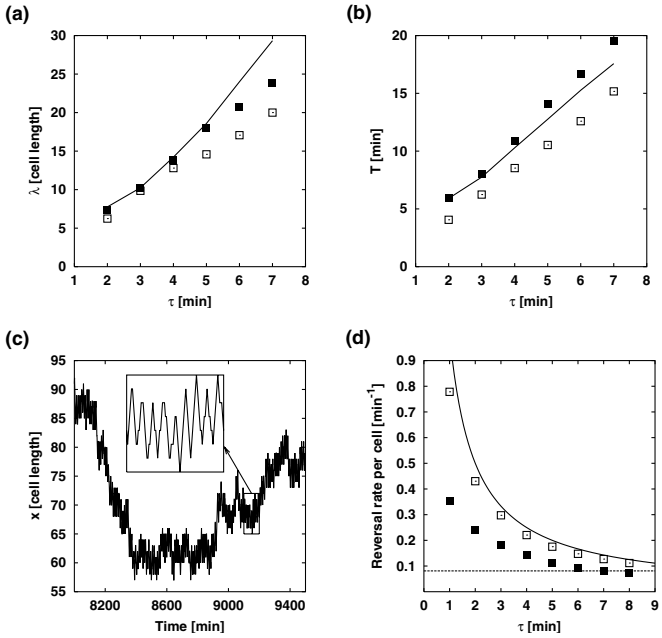

FIG. 4. Ripple wavelength λ (a) and period T (b) versus refractory time τ for 2D simulations (solid squares), 3D simulations (open squares), and 2D mean-field theory (solid line). (c) Single cell track with an enlargement of the marked region. (d) Reversal frequency against refractory time in 2D simulations (solid squares) and 3D simulations (open squares) compared to experiment (dotted line) and largest possible value $r_{\max}$ (solid line).

half a wavelength before they reverse their orientation [see Fig. 4(c)]. We measured the average reversal frequency of individual cells in the simulations taking advantage of the discrete, particle-based nature of our model. A typical trajectory of an individual cell in the model is displayed in Fig. 4(c). Most of the time, the cells in the model ride with the ripple crest and get reflected when two crests collide. Occasionally a cell ''tunnels'' through and continues a longer way with the same crest. The dependence of the mean reversal frequency on the refractory time τ is shown in Fig. 4(d) for 2D and 3D simulations. The reversal frequency is considerably larger in 3D due to the larger interaction neighborhood. For refractory times between 4 and 5 min, we measure mean reversal frequencies of ca. 0.2 per cell per minute in 3D (0.13 per cell per minute in 2D) in rough agreement with the experimentally observed values of ca. 0.1 reversals per cell and minute [20].

While previous experiments have not provided direct information about the duration of a refractory phase, measurements of reversal rates of myxobacteria exposed to high concentrations of isolated C-factor may give a first clue. Sager and Kaiser report an increased absolute reversal rate of roughly 0.3 reversals per cell per minute [20]. This can be interpreted as an upper bound for the reversal rate resulting from a refractory phase of ca. 3–4 min.

Mean-field theory.—Additional insight is obtained by deriving a mean-field theory of the discrete model in 2D. Such a description uses a hierarchy of rate equations in discrete time and space, which replace the discrete state variables by their average numbers. The mean-field scheme leads to the following set of 2τ equations:

$$\begin{aligned} r_1(x, t+1) &= r_1(x-1, t) - f_r(x-1, t) + r_\tau(x-1, t) \\ r_2(x, t+1) &= f_l(x-1, t) \\ &\vdots \\ r_\tau(x, t+1) &= r_{\tau-1}(x-1, t), \\ \\ l_1(x, t+1) &= l_1(x+1, t) - f_l(x+1, t) + l_\tau(x+1, t) \\ l_2(x, t+1) &= f_r(x+1, t) \\ &\vdots \\ l_\tau(x, t+1) &= l_{\tau-1}(x+1, t), \end{aligned} \tag{1}$$

where r_1 (l_1) are right (left) moving cells that can reverse, while $r_2, \ldots, r_\tau$ ($l_2, \ldots, l_\tau$) denote right (left) moving cells in the various stages of the refractory phase. The functions f_r and f_l describe the average numbers of reversals of right and left moving cells. From simple probability arguments we obtain

$$f_r(x,t) = \left\langle \frac{r_1(x,t) S_l(x+1,t)}{\max(S_r(x,t)+S_l(x,t), S_r(x+1,t)+S_l(x+1,t))} \right\rangle,$$
$$f_l(x,t) = \left\langle \frac{l_1(x,t) S_r(x-1,t)}{\max(S_r(x,t)+S_l(x,t), S_r(x-1,t)+S_l(x-1,t))} \right\rangle, \quad (2)$$

where $S_r(x,t) = \sum_{i=1}^{\tau} r_i(x,t)$ and $S_l(x,t) = \sum_{i=1}^{\tau} l_i(x,t)$. Since the number of particles on any given site is rather small, it is not sufficient to use their mean values in the reversal function which would be the standard approach for the derivation of, e.g., rate equations describing chemical reactions. Instead, one has to specify the distribution of the quantities l_1, r_1 around their mean values and sum over all possible states [indicated by the angle brackets in Eqs. (2)]. We have used Poissonian weights and performed a linear stability analysis of the homogeneous stationary state $r_1(x,t) = l_1(x,t) = \rho_S$ and $r_i(x,t) = l_i(x,t) = \rho_R$ for $i = 2, \ldots, \tau$. This state describes a flat layer of cells with equal amounts of left and right moving bacteria. The actual values of ρ_S and ρ_R depend on the parameters τ and $\bar{n}$ and obey $\rho_R = f_r(x,t) = f_l(x,t)$ and $\bar{n} = 2[\rho_S + (\tau - 1)\rho_R]$. For $\tau = 5$ and $\bar{n} = 3$, we find, for example, $\rho_S \approx 0.635$ and $\rho_R \approx 0.216$.

The linear stability analysis of the rate equations (1) with $\bar{n} = 3$ reveals a linear instability of this flat layer state against an oscillatory instability with finite wave number for $\tau \geq 4$ min (see eigenvalue curves in Fig. 5).

Moreover, we obtain the wave number k with the fastest growth rate for $\tau \geq 4$ min or with weakest damping for $\tau < 4$ min and the associated frequency ω as a function of the refractory time τ from the maxima of the curves in Fig. 5. A comparison of the corresponding wavelengths $\lambda = 2\pi/k$ and periods $T = 2\pi/\omega$ with equivalent quantities extracted from a Fourier analysis of simulation data of the 2D model shows good agreement below and near the threshold $\tau \leq 4$ min [see Figs. 4(a) and 4(b)]. Above the threshold, nonlinear effects lead to a deviation of the predictions from linear stability analysis.

Summary.—We present a discrete model for the formation of standing wave ripple patterns during the aggregation of myxobacteria. The reversal mechanism of cells following collisions has to be supplemented by a refractory phase that specifies a minimum time between subsequent reversals. The duration of this phase determines the wavelength and the period of the ripple pattern. The "microscopic" single cell behavior in the discrete model agrees well with the experiments on the reversal frequency of cells in [20]. Recent experiments show also traveling wave rippling patterns [21], which have been modeled with continuous models derived from similar assumptions to the ones described here [22,23]. Our study strongly suggests further experiments of single cell motility to verify the refractory hypothesis and to elucidate its biochemical basis. Moreover, myxobacterial rippling provides the first example of pattern formation mediated by migration and direct cell-cell interaction, which may also be involved in myxobacterial fruiting body formation as well as self-organization processes in other multicellular systems.

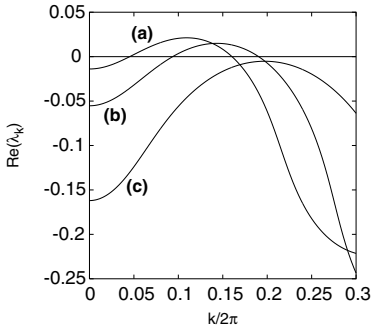

FIG. 5. Numerically obtained real part of eigenvalues for the linearization of Eqs. (1). Only the branch with the rippling instability is shown. Parameters: (*a*) $\tau = 5$ min, (*b*) $\tau = 4$ min, and (*c*) $\tau = 3$ min.

[1] E. Ben-Jacob, I. Cohen, and H. Levine, Adv. Phys. **49**, 395 (2000).
[2] E. O. Budrene and H. C. Berg, Nature (London) **349**, 630 (1991); **376**, 49 (1995).
[3] E. Ben-Jacob *et al.*, Nature (London) **368**, 46 (1994).
[4] G. Gerisch, Naturwissenschaften **58**, 430 (1971).
[5] P. Devreotes, Science **245**, 1054 (1989).
[6] F. Siegert and C. Weijer, J. Cell Sci. **93**, 325 (1989); Physica (Amsterdam) **49D**, 224 (1991); Curr. Biol. **5**, 937 (1995).
[7] W. F. Loomis, Microbiol. Rev. **60**, 135 (1996).
[8] *Chemical Waves and Patterns*, edited by R. Kapral and K. Showalter (Kluwer, Dordrecht, 1996).
[9] J. Martiel and A. Goldbeter, Biophys. J. **52**, 807 (1987).
[10] T. Höfer, J. A. Sherratt, and P. K. Maini, Proc. R. Soc. London B **259**, 249 (1995).
[11] L. Tsimring *et al.*, Phys. Rev. Lett. **75**, 1859 (1995).
[12] M. P. Brenner, L. S. Levitov, and E. O. Budrene, Biophys. J. **74**, 1677 (1998).
[13] J. K. Parrish and L. Edelstein-Keshet, Science **284**, 99 (1999).
[14] T. Vicsek *et al.*, Phys. Rev. Lett. **75**, 1226 (1995).
[15] H. J. Bussemaker, A. Deutsch, and E. Geigant, Phys. Rev. Lett. **78**, 5018 (1997).
[16] M. Dworkin, Microbiol. Rev. **60**, 70 (1996).
[17] L. J. Shimkets, Microbiol. Rev. **54**, 473 (1990).
[18] H. Reichenbach, Ber. Deutsch. Bot. Ges. **78**, 102 (1965).
[19] L. J. Shimkets and D. Kaiser, J. Bacteriol. **152**, 451 (1982).
[20] B. Sager and D. Kaiser, Genes Dev. **8**, 2793 (1994).
[21] R. Welch and D. Kaiser, Proc. Natl. Acad. Sci. U.S.A. **98**, 14 907 (2001).
[22] O. Igoshin *et al.*, Proc. Natl. Acad. Sci. U.S.A. **98**, 14 913 (2001).
[23] F. Lutscher and A. Stevens, J. Nonlinear Sci. (to be published).